AAV *cis*-regulatory sequences are correlated with ocular toxicity

Wenjun Xiong[a,b,1,2], David M. Wu[c,d,1], Yunlu Xue[c,1], Sean K. Wang[c], Michelle J. Chung[c,e], Xuke Ji[c,d], Parimal Rana[c,d], Sophia R. Zhao[c,e], Shuyi Mai[a,b], and Constance L. Cepko[c,e,2]

[a]Department of Biomedical Sciences, City University of Hong Kong, Kowloon, Hong Kong SAR, China; [b]Shenzhen Research Institute, City University of Hong Kong, Shenzhen 518057, China; [c]Department of Genetics, Harvard Medical School, Boston, MA 02115; [d]Retina Service, Massachusetts Eye and Ear Infirmary, Harvard Medical School, Boston, MA 02114; and [e]Howard Hughes Medical Institute, Chevy Chase, MD 20815

Contributed by Constance L. Cepko, January 27, 2019 (sent for review December 19, 2018; reviewed by Deniz Dalkara and Mark A. Kay)

Adeno-associated viral vectors (AAVs) have become popular for gene therapy, given their many advantages, including their reduced inflammatory profile compared with that of other viruses. However, even in areas of immune privilege such as the eye, AAV vectors are capable of eliciting host-cell responses. To investigate the effects of such responses on several ocular cell types, we tested multiple AAV genome structures and capsid types using subretinal injections in mice. Assays of morphology, inflammation, and physiology were performed. Pathological effects on photoreceptors and the retinal pigment epithelium (RPE) were observed. Müller glia and microglia were activated, and the proinflammatory cytokines TNF-α and IL-1β were up-regulated. There was a strong correlation between *cis*-regulatory sequences and toxicity. AAVs with any one of three broadly active promoters, or an RPE-specific promoter, were toxic, while AAVs with four different photoreceptor-specific promoters were not toxic at the highest doses tested. There was little correlation between toxicity and transgene, capsid type, preparation method, or cellular contaminants within a preparation. The toxic effect was dose-dependent, with the RPE being more sensitive than photoreceptors. Our results suggest that ocular AAV toxicity is associated with certain AAV *cis*-regulatory sequences and/or their activity and that retinal damage occurs due to responses by the RPE and/or microglia. By applying multiple, sensitive assays of toxicity, AAV vectors can be designed so that they can be used safely at high dose, potentially providing greater therapeutic efficacy.

AAV | gene therapy | toxicity | retina | retinal pigment epithelium

Adeno-associated viruses (AAVs) are small, single-stranded (ss) DNA viruses in the *Parvoviridae* family that have several advantages as somatic gene therapy vectors. Recombinant AAV genomes typically lack viral genes and do not efficiently integrate into the host genome, reducing the risk of insertional mutagenesis. They establish as stable episomes and express transgenes indefinitely in postmitotic cells. Naturally existing AAV variants, together with an array of engineered variants, can infect a large variety of tissues and cell types in both animals and humans (1–3). These capsid variants can enable more targeted infection of a selected set of cell types, with transgene expression further specified through the use of transcription regulatory sequences. Finally, AAV is nonpathogenic, even in its wild-type form, which has predicted its safety as a gene therapy vector. Multiple clinical trials have indeed borne this out (4–7).

AAV has emerged as the vector of choice for ocular diseases. There are many recessive disease genes (https://sph.uth.edu/retnet/), and complementation by a vector-encoded gene can lead to an improvement in vision (8, 9). The target cells for ocular gene therapy are most often the photoreceptors and retinal pigment epithelial (RPE) cells, as most genetic retinal diseases begin with dysfunction, often followed by death, of these cell types. There are two types of photoreceptors: rods, necessary for vision in dim light, and cones, required for color and daylight vision. Photoreceptor cells are supported by the RPE, a monolayer of epithelial cells with processes interdigitated with the outer segments (OS) of the photoreceptors. The subretinal space, the virtual space between the RPE and photoreceptors, is thus an effective injection delivery site for most ocular human gene therapy. In addition to these target cell types' being very accessible for gene therapy, the eye offers several other advantages for somatic gene therapy. It is relatively immune-privileged (10) and anatomically compartmentalized and can be targeted by established clinical interventions. Its target cells do not replicate and thus do not need integrating viruses. One further attribute that is particularly valuable, given the expense of generating pure viral vectors, is that only a small amount of virus is needed for local administration. These advantages stand in contrast to the systemic administration required for large organs, such as liver or muscle, and contributed to the approval of AAV encoding the RPE65 gene (Luxturna) for Leber's congenital amaurosis 2 (LCA2), a rare retinal disease (4–6). AAV has proven to be generally safe in the LCA2 clinical trials, as well as in several clinical trials for other ocular diseases, such as choroideremia and retinitis pigmentosa (11–13).

Despite the safety of the human trials to date, as AAV therapy expands to a larger number of patients and additional indications, problems may be unmasked. Current subretinal injections lead to infection only of cells near the injection site, which comprise a small percentage of target cells. A more complete infection would

Significance

Adeno-associated viral (AAV) gene therapy is becoming an important therapeutic modality, especially for ocular diseases, due to its efficiency of gene delivery and relative lack of pathogenicity. However, AAV sometimes can cause inflammation and toxicity. We explored such effects using injections into the mouse eye. We found a strong correlation of toxicity and inflammation with the use of promoters that were broadly active, or specifically active in the retinal pigment epithelium. AAVs with photoreceptor-specific promoters were found to be nontoxic at all doses tested. These studies reveal that safer vectors can be designed if assays for relevant and specific cell types are developed and tested with a range of vectors with different genomic elements.

Author contributions: W.X., D.M.W., Y.X., and C.L.C. designed research; W.X., D.M.W., Y.X., S.K.W., M.J.C., X.J., P.R., S.R.Z., and S.M. performed research; W.X., D.M.W., Y.X., S.K.W., M.J.C., X.J., P.R., S.R.Z., S.M., and C.L.C. analyzed data; and W.X., D.M.W., Y.X., and C.L.C. wrote the paper.

Reviewers: D.D., Université Pierre et Marie Curie; and M.A.K., Stanford University.

Conflict of interest statement: The authors note we have received funding from Astellas for our work.

[1]W.X., D.M.W., and Y.X. contributed equally to this work.

[2]To whom correspondence may be addressed. Email: wenjun.xiong@cityu.edu.hk or cepko@genetics.med.harvard.edu.

This article contains supporting information online at www.pnas.org/lookup/suppl/doi:10.1073/pnas.1821000116/-/DCSupplemental.

Published online March 4, 2019.

likely lead to a greater improvement in vision but would require a larger viral load, perhaps leading to toxicity. Toxicity associated with higher doses has been seen in animals, including nonhuman primates (NHPs), in both nonocular and ocular tissues. An early indication came from treatment of hemophilia B by AAV-mediated Factor IX expression. AAV infection in the liver triggered memory T cells reactive with the capsid, which cleared the infected cells and resulted in only transient expression of Factor IX (14). More recently, systemic delivery of high doses of an AAV variant to NHPs and pigs led to neurotoxicity, due to an uncharacterized mechanism (15). Specifically in the eye, AAV toxicity has been observed in both small and large animal models (16–18). For example, using AAV2-CNGA3 to treat color blindness (achromatopsia) in sheep, two animals had loss of photoreceptors and RPE, and one animal injected with a high dose showed both retinal atrophy and lymphocytic infiltration (19). In another study, AAV8-CNGA3 were subretinally injected into NHP eyes, and activation of both innate and adaptive immune responses were observed in the injected eyes despite concomitant steroid treatment (20). In one of the LCA2 gene therapy trials, strong evidence of an inflammatory response emerged. Five out of eight subjects injected with the higher dose of AAV2-RPE65 [1E12 vector genomes (vg) per eye] developed various degrees of intraocular inflammation (21). One significant adverse event was reported in the Alberta choroideremia gene therapy trial, in which presumed intraretinal inflammation led to permanent structural and functional impairment of the patient's treated retina (22).

We have been developing AAV gene therapy for retinal degenerations, hoping to create vectors that are able to deliver genes that can prolong photoreceptor survival and function independent of specific disease genes. We found that subretinal delivery of some, but not all, AAVs consistently induced cone OS shortening, reduction of the outer nuclear layer (ONL) where rods and cones reside, and dysmorphic RPE in mice. We began tracking many aspects of the preparations and vector structures and found no link between ocular toxicity and preparation methods, endotoxin level, cellular protein contaminants, or whether they were made in-house or at various core facilities. To search for the source of toxicity, we tested virus stocks with different *cis*-regulatory sequences, transgenes, and capsids. We found a strong correlation between the *cis*-regulatory sequences and toxicity. AAVs incorporating all broadly active promoters tested, including cytomegalovirus immediate-early promoter (CMV) (23), human ubiquitin C promoter (UbiC) (24, 25), and chicken beta actin promoter (CAG) (26), as well as an RPE-specific promoter (Best1) (27), were toxic. In contrast, vectors with photoreceptor-specific promoters tested, including human red opsin (RedO) (28, 29), human rhodopsin (Rho) (29, 30), human rhodopsin kinase (RK) (31), and mouse cone arrestin (CAR) (32), were not toxic. As might be expected, toxicity among the toxic group of vectors was associated with the dose. However, it is notable that administration of our highest doses of stocks of photoreceptor-specific vectors did not lead to toxicity. The RPE was more sensitive to virus toxicity than photoreceptors. Microglia activation and inflammatory cytokine expression were triggered by the toxic viruses. These data highlight the need to develop sensitive assays, specific to the organ and cell types that are being targeted, for each viral construct. Such assays will enable the design of vectors that can be used to safely deliver higher doses of vectors, potentially leading to both greater safety and efficacy.

Results

Photoreceptor Toxicity Is Correlated with Promoter Specificity. Serotype 8 AAV (AAV8) viruses expressing either GFP or no transgene ("null") under the control of different promoters were injected subretinally into neonatal mice (CD-1). Neonatal mice were used as we have been able to achieve complete infection of the RPE and retina using animals of this age (33). In addition, less tissue damage is induced, and/or is repaired, by injection at this early stage compared with the mature stage. The retinas and RPE were harvested for histological analysis at 30 d postinfection (or as indicated). The CMV promoter/enhancer sequence drives robust transgene expression in cone photoreceptors and the RPE, as well as other cell types (vector map shown in *SI Appendix*, Fig. S1) (33). AAV8-CMV-GFP induced photoreceptor toxicity and glial activation, indicated by cone OS shortening, ONL thinning, cone photoreceptor loss, and up-regulation of GFAP in retinal glial cells, the Müller glia (Fig. 1). In contrast, GFP expression driven by the photoreceptor-specific promoters, including RedO (28, 29), Rho (29, 30), RK (31), and CAR (29, 32), induced no retinal toxicity or glial activation (Fig. 1 and *SI Appendix*, Fig. S2). To determine if toxicity was due to protein expression, AAV8-CMV-null that did not express any transgene was tested. AAV8-CMV-null was just as toxic as AAV8-CMV-GFP (Fig. 1*C* and *SI Appendix*, Fig. S2).

RPE Toxicity Is Induced by AAV Vectors with Broadly Active Promoters and an RPE-Specific Promoter. Promoter-specific AAV toxicity also was observed in the RPE, which is efficiently transduced by subretinally delivered AAV. We developed a semiquantitative assay to measure the RPE toxicity level to compare among vectors. Whole RPE flatmounts were stained with phalloidin, which labels the f-actin borders of the hexagonal RPE array. These were imaged with a spinning-disk microscope and scored for the morphology, using a grading system with six grades that we devised. Grade 0 indicates completely normal RPE morphology and grade 5 indicates complete RPE loss (Fig. 2*A*). Four representative areas in the midperiphery of each flatmount were imaged and evaluated by four independent scorers who did not know the vector type/dose, with the average score for each flatmount shown in Fig. 2*B*. With this evaluation system, we found that the broadly active promoters, CMV, CAG, and UbiC, induced strong RPE toxicity, while none of the photoreceptor-specific promoters induced RPE toxicity (Fig. 2*B* and *SI Appendix*, Fig. S3). We also found that RPE damage is long-lasting and increases with time postinfection (*SI Appendix*, Fig. S4). The Best1 promoter was also tested for toxicity as it can drive strong expression in the RPE at a level comparable to that of CMV or CAG (27). Interestingly, AAV8 with Best1 promoter also induced RPE toxicity in the RPE (Fig. 2*B* and *SI Appendix*, Fig. S3). Table 1 shows a strong correlation between toxicity and the promoter used.

AAV Toxicity Was Not Found to Be Dependent on the Preparation Method. To determine if the preparation method contributed to AAV toxicity, several different AAV8 preparation and purification methods were tested by our laboratory. In addition, stocks of the same genomes and capsids were obtained from three different virus core facilities. In all cases, toxicity was observed. Furthermore, we examined toxic and nontoxic preparations on protein gels to examine the level of contamination by cellular proteins. We found that the level of cellular protein contaminants did not correlate with toxicity (*SI Appendix*, Fig. S5). Finally, endotoxin level in the plasmids for vector preps was unlikely to contribute to the toxicity as endotoxin-free plasmid prep kits were used. In addition, our test for endotoxin, and those of the core facilities, showed that endotoxin levels were very low in the preparations which were tested.

The Severity of Photoreceptor and RPE Toxicity Is Dependent upon the Dose of AAV. AAV vectors are injected subretinally at a wide range of doses (from 1E10 vg per eye to 1E12 vg per eye) in clinical trials (21, 22, 34, 35). To investigate whether AAV-induced toxicity is dose-dependent, we injected AAV8-CMV-GFP viruses at three doses (5E8, 1E9, and 2E9 vg per eye) into neonatal CD-1 mice. RPE toxicity was evaluated at 30 d postinfection. There was a clear

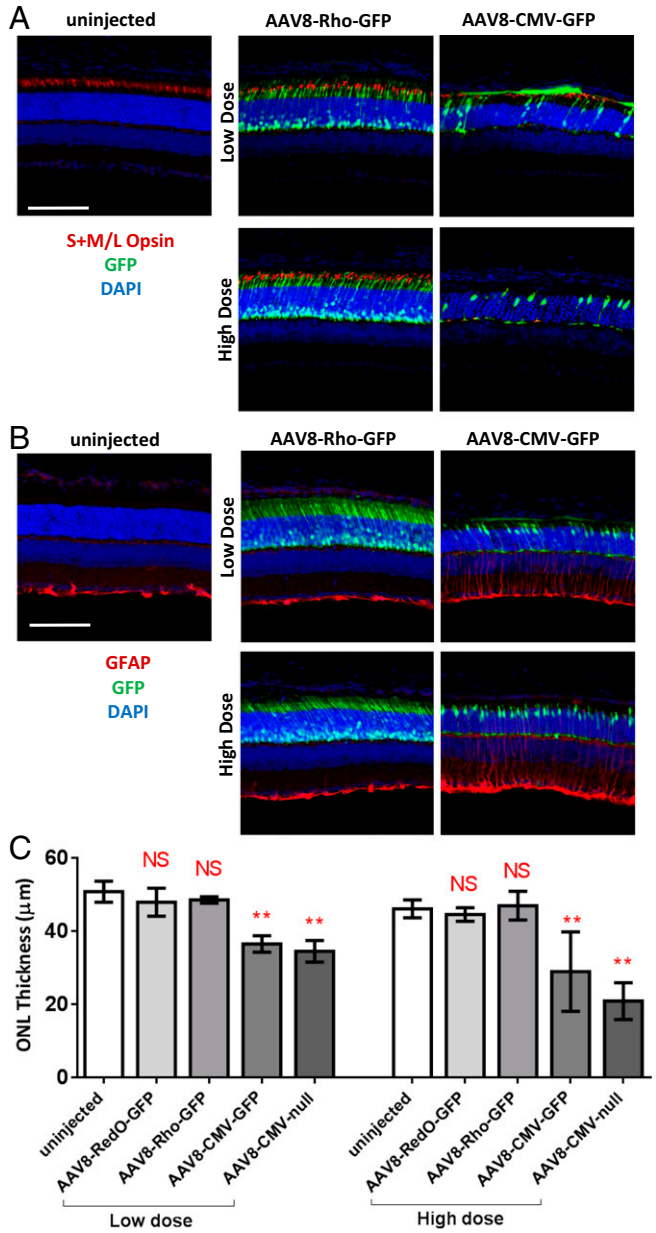

Fig. 1. Retina toxicity is induced by broadly active but not retinal cell-type-specific promoters. (*A* and *B*) Wild-type retinas of CD-1 mice were infected at P0 with the indicated viruses at either high (3E9 vg per eye) or low dose (8E8 vg per eye) and harvested at P30 for histology. Retinal cross-sections were stained for short- and medium/long-wavelength opsins (red) (*A*) and for GFAP (red) (*B*). Loss of opsin staining and up-regulated expression of GFAP were observed in the retinas infected with AAV8-CMV-GFP. (Scale bars, 100 μm.) (*C*) Quantification of ONL thickness at 1 mm from optic nerve head (ONH). Data are presented as mean ± SD. $n = 3$–17 per group. One-way ANOVA analysis with Tukey test, $^{**}P < 0.01$; NS, not significant between the designated group and the uninjected group.

correlation between the severity of toxicity to the RPE and virus dose. A lower dose of 5E8 vg per eye induced RPE cell enlargement with some loss of RPE cells (approximately grade 3), while a higher dose of 2E9 vg per eye caused nearly complete RPE loss (approximately grade 5) (Fig. 3 *A*–*C*).

Photoreceptor toxicity was examined in preparations where the RPE and retina were kept together, so that neighboring RPE and photoreceptor cells could be inspected for local effects. Cone OS were stained by peanut agglutinin (PNA), which was used as a proxy for overall photoreceptor health. Severe photoreceptor toxicity was seen at the doses of 1E9 and 2E9 vg per eye such that cone OS were largely absent (Fig. 3 *E* and *F*). However, photoreceptors were less sensitive to AAV toxicity than RPE, as AAV8-CMV-GFP–infected RPE demonstrated clear abnormalities in morphology at the low dose (5E8 vg per eye), while neighboring cone OS were largely normal (Fig. 3 *A* and *D*). RPE and cone OS loss were usually found in the same area, which could have resulted from higher local infection or an amplifying effect between compromised RPE and photoreceptors. Damage to the RPE and retina was always restricted to the infected area. When the entire retina/RPE was not infected, the toxicity did not spread beyond GFP-positive areas (*SI Appendix*, Fig. S6). These results show that the severity of RPE and photoreceptor toxicity is positively correlated with the dose of toxic

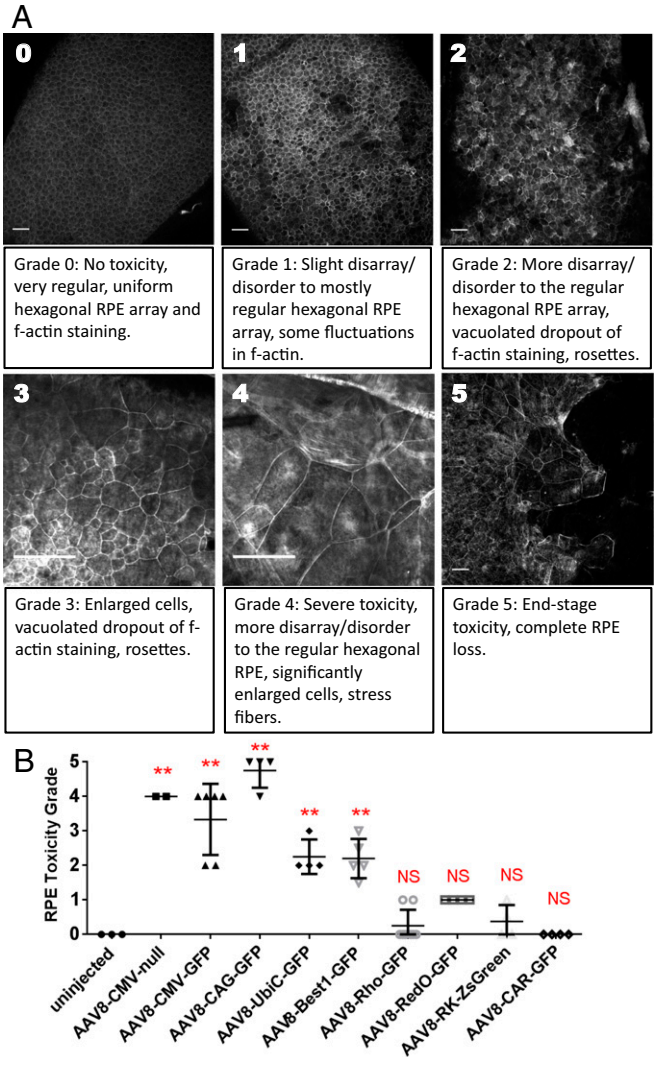

Fig. 2. RPE toxicity is induced by promoters that are active in the RPE. (*A*) Grading criteria of RPE toxicity, with grade 0 representing completely healthy RPE and grade 5 representing the most severe RPE damage. The typical phenotypes of each grade are described below each image. (Scale bars, 50 μm.) (*B*) Scatter dot plot of RPE toxicity grades. All viruses were tested at a dose of 8E8 vg per eye, except for AAV8-CAR-GFP (3E9 vg per eye), in CD-1 mice injected at P0 and killed at P30. Data are presented as mean ± SD. $n = 2$–8 per group. One-way ANOVA analysis with Tukey test, $^{**}P < 0.01$; NS, not significant between the designated group and the uninjected group.

Table 1. Summary of toxicity of all viruses tested in this study

Vector name/serotype	Promoter/regulatory sequence full name (refs.)	Vector origin	Toxicity to retina	Toxicity to RPE
AAV8-CMV-GFP	CMV immediate-early promoter and enhancer (23)	Harvard vector core (Addgene no. 67634)	Y	Y
AAV5-CMV-GFP	As above	As above	Y	Y
AAVAnc80-CMV-GFP	As above	As above	Y	Y
AAV7m8-CMV-GFP	As above	As above	Y	Y
AAV8-CMV-null	As above	Harvard vector core (pAAV-MCS8)	Y	Y
AAV8-UbiC-GFP	Human UbiC promoter (24, 25)	Substituted CMV in pAAV-CMV-GFP with UbiC promoter (Addgene no. 11155)	L	Y
AAV8-CAG-GFP	CMV immediate-early enhancer + chicken beta actin promoter (26)	E. Boyden laboratory (Addgene no. 37825)	Y	Y
AAV8-RedO-GFP	Human red opsin (28)	B. Roska laboratory (29)	N	N
AAV8-Rho-GFP	Human rhodopsin (30)	B. Roska laboratory (29)	N	N
AAV8-CAR-GFP	Mouse cone arrestin promoter (32)	B. Roska laboratory (29)	N	N
AAV8-RK-ZsGreen	Human rhodopsin kinase (31)	T. Li laboratory (31)	N	N
AAV8-Best1-GFP	Human Bestrophin 1 (27)	Cloned into AAV vector by C.L.C. laboratory	L	Y

Toxicity to the retina was assessed by the immunohistological assays shown in Figs. 1 and 6*A*. Toxicity was defined by ONL thinning, loss of S+M/L opsin, GFAP up-regulation, and Iba1+ cell infiltration into the ONL, while low toxicity in the retina was defined as Iba1+ cells in the ONL and GFAP up-regulation without ONL thinning. Toxicity to the RPE was assessed by the 0–5 grading method on RPE flatmounts shown in Fig. 2, and toxicity was defined as a score >1. Nontoxic means that retina and RPE were indistinguishable from the uninjected controls. All viruses were tested at a dose of 8E8 vg per eye, except for AAV8-CAR-GFP (3E9 vg per eye). L, low toxicity; N, nontoxic; Y, toxicity.

virus, and that photoreceptors are more tolerant of AAV than the RPE. AAV vectors with photoreceptor-specific promoters did not induce toxicity even at the highest doses we were able to inject.

AAV Toxicity Manifests Across Mouse Strains and Is Associated with Multiple Capsid Types. To test whether toxicity is associated with a serotype other than type 8, we tested additional capsid types for transmission of a toxic genome. We also tested an additional mouse strain and expanded the type of assay to include clinically relevant in vivo imaging, using a fundus camera, and using optical coherence tomography (OCT), which can detect alterations in retinal and RPE structure. Postnatal day 0 (P0) mice were injected with AAV5, another commonly used capsid type, carrying CMV-GFP at a low dose (8E8 vg per eye) and a high dose (3E9 vg per eye) or AAV8-CMV-GFP as a positive control for toxicity. To test a mouse strain that avoids some of the light sensitivity of albino strains, such as the CD-1 strain, we injected the pigmented C57BL/6J strain. This pigmented strain was chosen as it is free of *rd8* and *cpfl3* mutations, which can lead to morphological and functional deficits in the retina (36, 37). As an initial measure of infection and to assess potential injection trauma, we used a fundus camera with a fluorescent light source to image GFP and eye morphology (Fig. 4*A*). Eyes receiving a low dose of AAV8-CMV-GFP or AAV5-CMV-GFP showed a variable degree of GFP expression in the RPE cells (Fig. 4*A*), similar to that observed in cross-sections (*SI Appendix*, Fig. S7) and flatmounts. Sparse GFP+ RPE cells were observed following infection of AAV8-CMV-GFP or AAV5-CMV-GFP at high dose, presumably due to death of RPE cells (Fig. 4*A* and *SI Appendix*, Fig. S7). Eyes injected with a nontoxic preparation of AAV8-CAR-GFP showed uniform distribution of GFP in photoreceptors (Fig. 4*A*). We also injected a mixture of two viruses, AAV8-RedO-GFP and AAV8-Best1-GFP (at a ratio of 5:1) to mimic the expression pattern of toxic CMV-GFP (i.e., RPE, most cones and some rods) to determine if this mixture of expression patterns might trigger toxicity. The GFP pattern of this combination gave bright RPE expression and uniform photoreceptor labeling and looked distinctly different from the toxic CMV-GFP (Fig. 4*A*). Using OCT, similar observations were made. Largely normal retinal layers were seen following infection with both low and high doses of AAV8-CAR-GFP or the combination of AAV8-RedO-GFP +AAV8-Best1-GFP (Fig. 4*B*). In contrast, infection with the low dose of AAV8-CMV-GFP or AAV5-CMV-GFP resulted in diminished outer limiting membrane (OLM) and inner segment/outer segment bands, created disturbances in the RPE bands, and led to intrusions into the subretinal-RPE space (Fig. 4*B*). Such intrusions may represent infiltrating immune cells (arrows in Fig. 4*B*, *Upper*). At high dose, infection with AAV8-CMV-GFP or AAV5-CMV-GFP resulted in more dramatic OCT manifestations with decreased ONL thickness and larger subretinal intrusions (Fig. 4*B*, *Lower*). Overall, these in vivo imaging results correlate well with our observations of toxic effects on photoreceptors and the RPE seen in histological preparations (Figs. 1 and 2 and *SI Appendix*, Fig. S7).

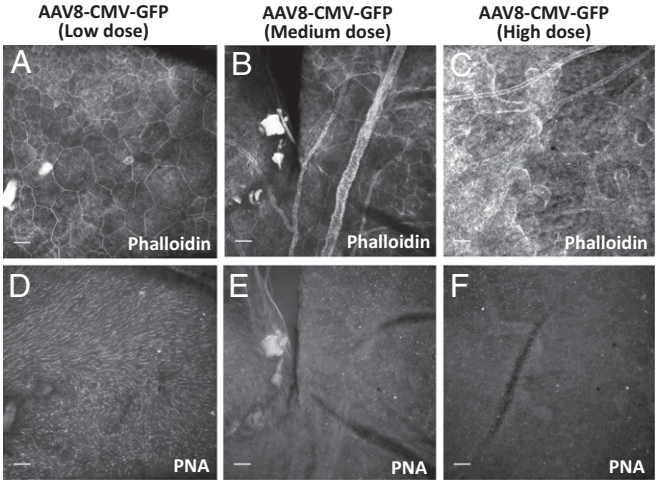

Fig. 3. RPE and retina damage is dose-dependent. Representative images of RPE and retina of P30 CD-1 mice following infection at P0 with low dose (5E8 vg per eye), medium dose (1E9 vg per eye) and high dose (2E9 vg per eye) of AAV8-CMV-GFP. (*A*–*C*) The RPE (labeled with phalloidin staining) and (*D*–*F*) photoreceptors (labeled with PNA) from the same areas are shown in upper and lower panels. (Scale bars, 50 μm.)

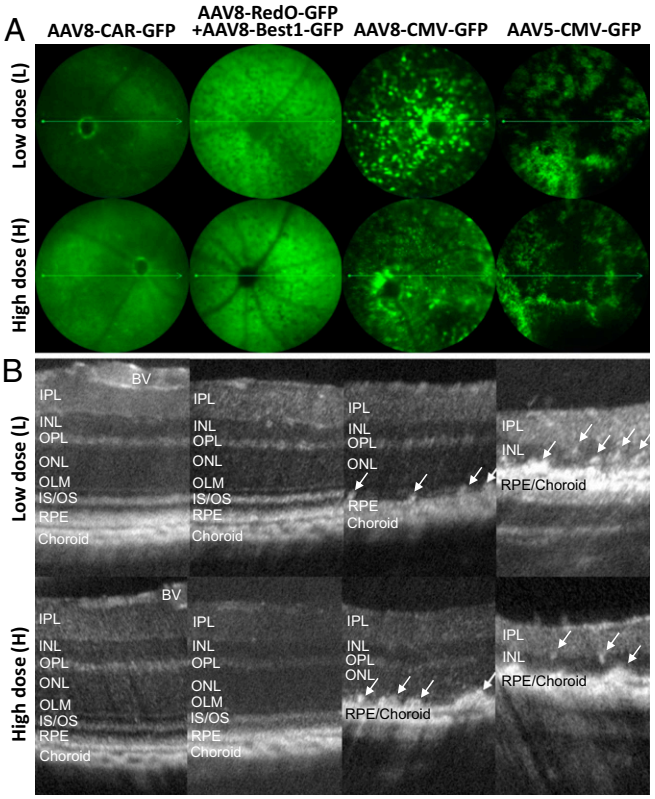

Fig. 4. OCT images of eyes infected by AAV8-CMV-GFP and AAV5-CMV-GFP. (*A*) Funduscopic images of eyes from C57BL/6J mice infected at P0 with low (L: 8E8 vg per eye) and high (H: 3E9 vg per eye) doses of AAV8-CAR-GFP, AAV8-RedO-GFP + AAV8-Best1-GFP (5:1 ratio), AAV8-CMV-GFP, and AAV5-CMV-GFP viruses. Infected mouse eyes were examined at approximately P30. Green arrow labels the plane where the OCT image was taken. (*B*) OCT images of the eyes shown in *A*. White arrowhead, intrusions in subretinal space. BV, blood vessel; INL, inner nuclear layer; IPL, inner plexiform layer; IS/OS, junction of inner and outer segments of photoreceptors; OPL, outer plexiform layer.

We also tested two engineered capsid types. AAV-CMV-GFP was packaged in Anc80, a capsid engineered to be less effectively neutralized by prior exposure to extant AAVs (3). Toxicity was also seen with AAVAnc80-CMV-GFP (Table 1). An AAV2 capsid derivative, 7m8, was developed for use in intravitreal injections, that is, injections into the cavity within the eyeball on the opposite side of the retina from the subretinal space (2). Intravitreal injections are used routinely and safely for the delivery of drugs for age-related macular degeneration. However, we tested the 7m8 capsid using subretinal injections, rather than intravitreal, to keep the injection site constant among vectors tested. AAV7m8-CMV-GFP also was toxic (Table 1). As we observed toxicity using AAV8, AAV5, Anc80, and 7m8, toxicity was not restricted to a particular capsid type.

Assessment of AAV Toxicity Using Clinical Measures of Visual Activity. Human vision can be assayed physiologically using electroretinograms (ERGs) under lighting conditions that assess rod versus cone function. Vision in animals can additionally be measured by a behavioral test, the optomotor assay. These assays were applied to C57BL/6J mice injected with AAV8-CMV-GFP viruses at P0. For nontoxic controls, mice were injected with the combination of AAV8-RedO-GFP and AAV8-Best1-GFP (again at a 5:1 ratio of RedO to Best1). Animals were first assessed for whether or not the injection was successful and nontraumatic by fluorescent fundus microscopy at approximately P21. For assessment of rod function and the downstream retinal pathway from rods, scotopic conditions (low light levels without background light) for the ERG were used, while for cone and cone pathway function, photopic conditions (with background light to saturate the rods) were used. The a-wave provides a measure of photoreceptor function, while the b-wave provides a measurement of ON-bipolar cell activity that also indicates the level of synaptic signaling between photoreceptors and their synaptic partners, the bipolar cells. Injection of the high dose of AAV8-CMV-GFP resulted in a significant drop in the a-wave (−84%, $P < 0.001$) and b-wave amplitudes (−71%, $P < 0.0001$) in scotopic conditions (Fig. 5 *A* and *B*), suggesting a severe functional deficit in rods and the rod pathway. Under photopic conditions, the AAV8-CMV-GFP–injected groups showed a 50–70% decrease in b-wave amplitudes at all light intensities (Fig. 5 *C* and *D*), compared with the group injected with the combination of AAV8-RedO-GFP plus AAV8-Best1-GFP, and an approximately fivefold increase in $I_{1/2}$ (Fig. 5*D*, *Inset*), a measure of the flash intensity giving 50% maximal response (38). These observations indicate that the cones or cone pathway in the animals injected with AAV8-CMV-GFP were much less sensitive to light as they required fivefold more photons to reach the 50% maximal response.

Injected mice also were tested in the optomotor assay, which measures visual acuity by assessing the motor response of mice under photopic conditions to a virtual rotation of stripes of different widths (39). In keeping with the results of the photopic ERG, the optomotor assay showed a deterioration in photopic vision, with visual acuity decreased by 30% ($P < 0.05$) in the high-dose AAV8-CMV-GFP group (Fig. 5*E*), consistent with a decrease in cone function.

Although mice injected with the low dose of AAV8-CMV-GFP had milder perturbations than mice injected with the high dose, significant differences between animals injected with toxic and nontoxic AAV preparations persisted. The scotopic ERG a-wave amplitude was 49% lower ($P < 0.05$) in mice injected with low-dose AAV8-CMV-GFP than in mice injected with the combination of AAV8-RedO-GFP and AAV8-Best1-GFP (Fig. 5*B*). The scotopic b-wave implicit time was significantly delayed (27 ms slower than control, $P <$ 1E-8) (Fig. 5*B*). In addition, the photopic ERG showed that the $I_{1/2}$ of the low-dose AAV8-CMV-GFP–injected eyes was approximately twofold higher (i.e., twofold less sensitive to light) than that of eyes injected with the same dose of AAV8-RedO-GFP plus AAV8-Best1-GFP (Fig. 5*D*, *Inset*). These results demonstrate that the retinal damage induced by AAV8-CMV-GFP toxicity can result in visual deficits, in correlation with the dose of administered virus.

Microglia Activation Is Associated with AAV-Induced Toxicity. Microglia are the main innate immune cell type in the retina (40). We examined whether they were activated in retinas infected with AAV at 30 d postinfection. Iba1 is a marker of microglia and increases in intensity with activation (41). We examined Iba1 staining and found that there were significantly more Iba1-positive microglia in the retina after infection with high-dose (3E9 vg per eye) AAV8-CMV-GFP (Fig. 6*A*). Activated microglia migrated to the ONL and subretinal space, where they adopted an amoeboid or activated morphology (Fig. 6*A* and *SI Appendix*, Fig. S8*A*). In contrast, microglia number, localization, and morphology did not change significantly in retinas infected with AAV8-RedO-GFP (Fig. 6 *A* and *B*). Microglia responses were very sensitive to toxic viruses, as their activation was evident in low-dose (8E8 vg per eye) AAV8-CMV-GFP–infected retinas (Fig. 6*B* and *SI Appendix*, Fig. S8*A*). To confirm the increase of microglia, we examined microglia numbers using a transgenic mouse strain, Cx3cr1-GFP, in which microglia are marked by GFP (42). This strain was injected with AAV8-CMV-TdTomato (3E8 vg per eye), which utilizes the

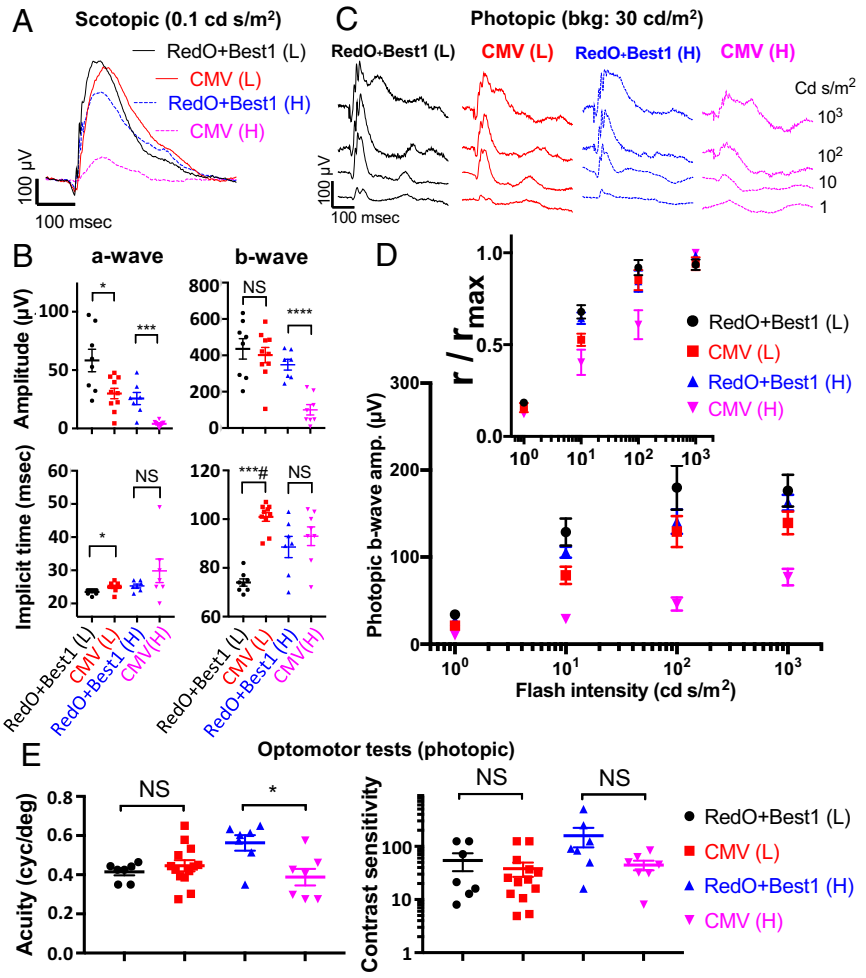

Fig. 5. Toxic AAV causes ERG and optomotor manifestations in C57BL/6J mouse eyes. (*A*) Representative trace of scotopic ERG (flash intensity: 0.1 cd s/m^2, wavelength: 530 nm) of P30 eyes injected at P0 with AAV8-RedO-GFP + AAV8-Best1-GFP (5:1 ratio, RedO+Best1) or AAV8-CMV-GFP (CMV) at low dose or high dose. (*B*) Statistics of scotopic ERG parameters (a-wave and b-wave amplitude and implicit time) of P30 eyes injected at P0 with RedO+Best1 (low dose: $n = 8$, high dose: $n = 7$) and CMV (low dose: $n = 10$, high dose: $n = 8$). (*C*) Representative traces of photopic ERG of P30 eyes injected at P0 with RedO+Best1 and CMV, elicited by 1 (peak), 10 (peak), 100 (xenon), and 1,000 (xenon) cd s/m^2 white light flashes with a white light background (bkg) of 30 cd/m^2. (*D*) Ensemble-averaged photopic ERG b-wave amplitude from P30 eyes injected at P0 with RedO+Best1 (low dose: $n = 8$, high dose: $n = 7$) and CMV (low dose: $n = 10$, high dose: $n = 8$). Significance (*P* value): CMV (H) vs. RedO+Best1 (H) at 1 (****), 10 (*#), 100 (****), and 1,000 (****) cd s/m^2; CMV (L) vs. RedO+Best1 (L) at 1 (**), 10 (*), 100 (NS), and 1,000 (NS) cd s/m^2. (*Inset*) The normalized photopic ERG b-wave intensity–response (r/r_{max}) curves with $I_{1/2}$ of RedO+Best1 (low dose: 4.8 cd s/m^2, high dose: 5.8 cd s/m^2), and CMV (low dose: 9.0 cd s/m^2, high dose: 27.0 cd s/m^2). (*E*) Photopic optomotor responses from approximately P35 eyes injected either with RedO+Best1 (low dose: $n = 7$, high dose: $n = 7$) or CMV (low dose: $n = 13$, high dose: $n = 7$). Acuity: tested at 100% contrast; contrast sensitivity: tested at 0.128 cyc/deg and 1.5-Hz temporal frequency. For all panels, data are presented as mean ± SEM, unpaired Student's *t* test $^*P < 0.05$, $^{***}P < 0.001$, $^{****}P < 0.0001$, $^{*\#}P < 1 \times 10^{-6}$, $^{***\#}P < 1 \times 10^{-8}$; NS, not significant. CMV, AAV8-CMV-GFP; H, high dose; L, low dose; RedO+Best1 for AAV8-RedO-GFP +AAV8-Best1-GFP (5:1 ratio).

same CMV enhancer/promoter as the toxic AAV8-CMV-GFP. The percentages of all live retinal cells that were GFP+ microglia were analyzed using flow cytometry. A threefold increase of GFP+ microglia was observed in the AAV8-CMV-Tdtomato–infected retinas compared with uninjected or PBS-injected retinas (Fig. 6*C*).

Activated microglia, and potentially other cell types, may increase their expression of proinflammatory cytokines, such as TNF-α, IL-1β, IL-6, and/or IFN-γ. We tested this possibility by examining the levels of RNA for these genes by qPCR in the dissected retinas at 30 d postinfection. TNF-α and IL-1β were highly up-regulated in retinas infected with the toxic viruses, while the levels of IL-6 and IFN-γ were not significantly changed (Fig. 6*D*). The increase of TNF-α and IL-1β expression correlated with the dose of the injected toxic viruses (Fig. 6*D* and *SI Appendix*, Fig. S8*B*).

Discussion

Ocular delivery of AAV vectors is relatively safe, as shown by the results of several clinical trials (4, 6, 7, 43–45). Subretinal injection of AAV is the route used to administer virus for treatment of LCA, retinitis pigmentosa, and choroideremia (11, 22, 35). However, the sensitive assays that we were able to conduct in mice have shown that there can be several manifestations of toxicity from subretinal injections of AAV. Toxicity was seen with more than one type of capsid and did not correlate with preparation methods, endotoxin level, nonviral protein contamination, or mouse strain. The lack of correlation with preparation method is in agreement with the results from previous studies (46, 47). The two variables showing the strongest association to toxicity were the promoter and the viral dose. It is likely that other variables can contribute to toxicity in other cases (e.g., stocks with a high degree of endotoxin, or perhaps empty capsids,

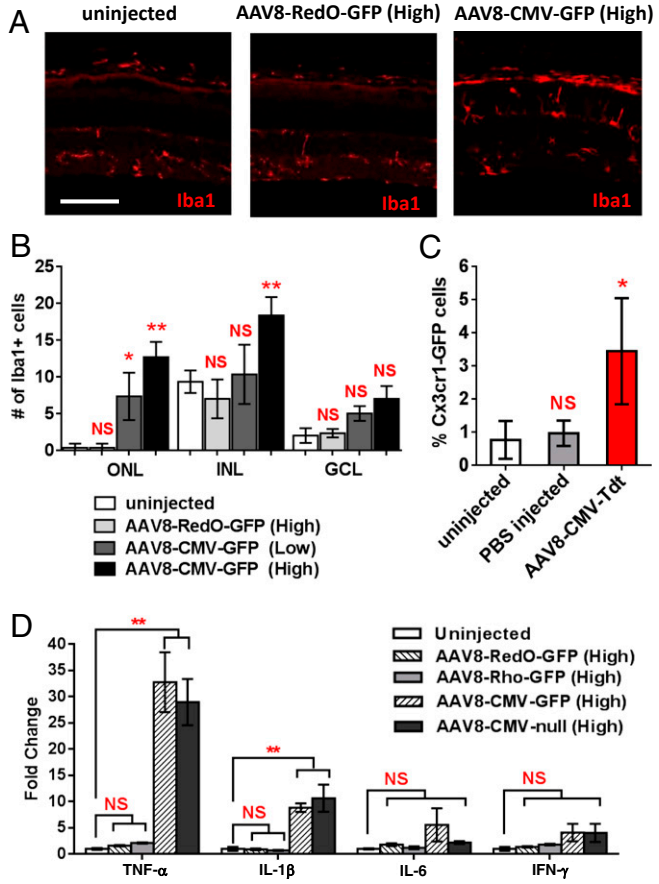

Fig. 6. Activation of microglia and innate immune response by toxic AAVs. (*A*) Iba1 staining of retinal sections from P30 eyes of CD-1 mice infected at P0 with the indicated AAV viruses at a dose of 3E9 vg per eye. (Scale bar: 50 μm.) (*B*) Quantification of displaced Iba1-positive cells by cell layer. High dose (3E9 vg per eye); low dose (8E8 vg per eye). Values are shown as mean ± SD. $n = 4$ per group. (*C*) Quantification of microglia in retinas of P20 Cx3cr1-GFP mice by flow cytometry injected with PBS or 3E8 vg per eye AAV8-CMV-TdTomato ($n = 3$–4 for all groups). Values are shown as mean ± SD. (*D*) Relative mRNA levels of TNF-α, IL-1β, IL-6, and IFN-γ by qPCR in the retinas of P30 CD-1 mice infected at P0 with the indicated AAV viruses at high dose (3E9 vg per eye). Expression level was normalized to *gapdh*. Values are shown as mean ± SEM. $n = 4$–8 per group. One-way ANOVA analysis with Tukey test, $^{**}P < 0.01$; $^{*}P < 0.05$; NS, not significant between the designated group and the uninjected group.

may be problematic). Our results show the importance of sensitive and organ-specific assays for different manifestations of toxicity. Ophthalmologists can use standard examination equipment to employ familiar consensus language and grading scales developed for clinical studies of uveitis (48). OCT, autofluorescence, and microperimetry are routinely used in preoperative planning for human gene therapy in the eye. In the posttreatment follow-up period, these modalities can then be used to quantitate changes from baseline across many parameters including retinal layer thickness, number of inflammatory cells (OCT), RPE viability and stress (autofluorescence), and retinal sensitivity (microperimetry) (49, 50). These strategies would allow for the development of safer vectors, reducing the likelihood of problems as a greater number of patients are treated.

In human clinical trials, the dose of AAV used in subretinal injections ranges from 1E10 vg per eye to 1E12 vg per eye (21, 22, 34, 35). So far, most ocular gene therapy trials have used AAV2, and thus less is known about the safety and efficacy of AAV8 or other capsid types. However, AAV8, and likely other capsid types under development, offer advantages in terms of number of cells, and/or the cell types, infected. In our study, AAV8 encapsidated toxic genomes were toxic at a dose of 5E8 vg per eye or higher. A recent study, also conducted by subretinal injections in mice, reported similar dose-dependent AAV retinal toxicity. They showed that AAV8-CAG-GFP at a dose of 5E9 vg per eye and above were toxic (18). Interestingly, they observed toxicity using a rhodopsin promoter to drive GFP. The dose that led to this toxicity was 1E11 vg per eye, which was 30-fold higher than our highest dose of a vector using a rhodopsin promoter. As dose is an important variable, the higher dose may be the reason for the toxicity of the AAV-Rho-GFP. In fact, it is difficult to extrapolate and compare results across studies, as different subjects/animals, injection routes, and age at injection are used. We used the somewhat unusual time point of P0 for our injections, but this is unlikely to be the cause of the toxicity that we observed. In collaborative studies using pigs, where injections were done to animals at 2 to 3 mo of age, toxicity also was seen using AAV8-CMV-GFP.* Moreover, other studies reporting ocular toxicity used injections into adults (16–21). One other variable making it difficult to compare among studies is the vexing issue of titer. Different groups use different methods to titer, and even for a given stock large differences can be reported, as was well illustrated in a trial where multiple groups measured the titer of the same stock, with differences of up to 100-fold reported (51). Toxic doses for different AAV serotypes are unlikely to be the same, as the cellular tropisms of different AAV serotypes can vary greatly (52). In fact, we noticed a correlation in toxicity among different capsids carrying toxic genomes and the degree of RPE infectivity, with AAV5 > AAV8 > AAV2. Overall, our results, and those of others (15, 16, 18), emphasize the importance of testing the dose of specific vectors with sensitive assays of several phenotypic aspects of relevant cell types. Most assays conducted to date examine only a few parameters, such as neutralizing antisera or gross inflammation and tissue damage.

In light of clinical trials conducted in the eye, it is interesting that two promoters shown to be toxic in our studies have been used safely in humans. The Best1 (also called VMD2) promoter has been used to express the RPE gene, MERTK, to treat one form of retinitis pigmentosa (11, 53). The AAV2-VMD2-hMERTK vector, when administered at 4E8 or 4E9 vg per eye in Sprague-Dawley rats, did not cause any obvious retinal damage compared with the saline-injected eyes (53). Of note, they did not examine RPE morphology in flatmount preparations, which may be a more sensitive measure of RPE stress. In the follow-up clinical trial, six patients who received either 5.9E10 vg or 1.8E11 vg of AAV2-VMD2-hMERTK vector did not develop severe complications (11). However, in patients with MERTK mutations there is defective RPE phagocytosis, and geographic atrophy existed at baseline. In these patients, there was an expansion of perifoveal atrophic areas, regardless of whether the eye received AAV2-VMD2-hMERTK. Intervention late in the course of the disease, and the fact that a phase I study is not designed to test for efficacy, may have been the reasons that atrophy was not arrested, as suggested by the authors. However, it is also possible that a rescue effect of the VMD2-hMERTK vector was blunted by RPE toxicity. In our study, we used an assay to specifically examine RPE morphology with administration of AAV8-Best1-GFP (8E8 vg per eye) and found that it showed toxicity for mouse RPE cells. Reducing the level of AAV8-Best1-GFP to 1E8 vg per eye, as in the nontoxic low-dose group, minimized toxicity while still providing a good level of GFP expression in the RPE (Fig. 4). In addition to the

*Chan et al., American Society of Gene & Cell Therapy (ASGCT) Annual Meeting, May 16–19, 2018, Chicago, IL, 1001 (abstr).

Best1 promoter in use in human trials, the CAG promoter is used in the LCA2 vector, Luxturna, approved by the Food and Drug Administration, using a dose that minimizes toxicity (6). However, since subretinal infections of human eyes result in local infection of ~10% of retinal or RPE cells, the clinical benefits are more limited than what would be ideal. If safer vectors could be developed a greater number of cells could be transduced, likely creating greater benefit to the patients, and the concern for safety could be lowered for all injections.

As discussed above, a key observation in our study is that toxicity correlated with promoter type, with the broadly active promoters and an RPE-specific promoter leading to toxicity, and photoreceptor-specific promoters being benign. Toxicity also has been seen with broadly active promoters, and not with cell-type–specific promoters, in other tissues, including the heart (54, 55) and the central nervous system (56, 57). However, a systematic investigation of several of each type of promoter has not been reported. One mechanism that might explain toxicity is that the broadly active promoters tend to drive higher expression of transgenes than cell-type–specific promoters. GFP protein has been shown to be toxic via reactive oxygen species and apoptosis (58, 59). However, toxicity cannot be solely attributed to GFP or any other transgene protein, as AAV8-CMV-null is as toxic as AAV8-CMV-GFP (Figs. 1 and 2), and other non-GFP proteins were seen to be toxic when expressed by CMV or CAG AAV vectors. Another hypothesis is that the CMV sequence, present in both the CMV and CAG vectors, stimulates an innate immune response, as CMV is a virus that activates the innate immune system naturally (60). Arguing against this, the UbiC and Best1 promoters are human in origin and also were toxic. Another possibility is that there is a common sequence motif among the toxic vectors. Toll-like receptor 9 (TLR9), which senses unmethylated CpG DNA, can detect the AAV genome and set off innate and adaptive immune responses (61), and CpG-depleted AAV vectors can evade TLR9-mediated immune detection (62). We examined the set of viruses that we tested and failed to find any correlated sequence motifs. A search for toxic sequences using deletions and chimeric viral genomes may be better able to detect toxic and/or protective sequences. In addition to innate immune sensing of DNA sequences, capsids also can be sensed, as TLR2, which is on the cell surface, can sense AAV2 and AAV8 capsids in Kupffer cells and liver sinusoidal endothelial cells (63). All capsids tested here led to toxicity when used to encapsidate toxic genomes but did not lead to toxicity when used to package nontoxic genomes, arguing against capsids alone stimulating toxic responses, at least at the doses tested here.

In addition to the sequence of an AAV genome, other aspects of an AAV genome may contribute to toxicity. The study of retinal toxicity by Khabou et al. (18) used a self-complementary (sc) AAV8-Rho-GFP, which was toxic at a high dose, while we did not observe toxicity using an ss AAV8-Rho-GFP, although it was tested at a much lower dose. Previous studies have shown that the double-stranded genome of scAAV can trigger a stronger immune response than ssAAVs, at least in part by activating the TLR9 pathway (64, 65). Further studies with scAAV vs. ssAAV using other cell-type–specific promoters and a wider range of doses will provide more insight into the correlation between toxicity and this aspect of genome structure.

It is of interest to consider the cell types that might be sensing the virus. The RPE and microglia are good candidates for this function. The RPE is situated between the rich vascular bed of the choriocapillaris and the retina, constitutes a portion of the blood-retinal barrier, and expresses at least several genes of the innate immune system, including the TLRs (66–68). Our observations favor a model in which the RPE is a primary sensor of toxic vectors, as all toxic vectors had promoters that were active within the RPE, including the RPE-specific promoter, Best1. The other two retinal glial cell types, Müller glia and astrocytes, are possible sensors of virus, as they also can respond to inflammatory stimuli (69–71). However, Müller glia are not yet born at P0 when we inject virus, and astrocytes are just beginning to migrate into the retina at P0 (72). However, it is possible that the inflammation seen in other studies of AAV infection of the retina following vitreal injections (73, 74) was due to sensing by one or both of these cell types, or endothelial cells. These previous studies used injections into mature animals where these cell types would be present and very accessible to vitreally delivered virus. Microglia also can sense and respond to virus (75), and given their activation by the toxic, but not by the nontoxic viruses, it is likely that they are involved. We did not see GFP in microglia following infection with any virus, but it has been reported that they are difficult to infect in vivo (76). However, it could be that they are infectable, but that they shut down viral gene expression. Detection of viral genomes using the newer and more sensitive DNA FISH methods may resolve this issue (77, 78). The other cell types at the injection site, the retinal neurons, particularly photoreceptors, generally do not express genes encoding sensors of innate immunity (79–82) and thus would not be expected to react directly to viral transcription and/or RNA.

What is being sensed in the RPE and/or microglia? Our data are consistent with transcription from a nonchromosomal genome, which, if true, would be a novel mechanism, and/or some form of viral RNA. The ITRs in AAV vectors have been shown to have promoter activity (83, 84). If an ITR generates an antisense transcript, it could hybridize to a sense transcript, creating double-stranded RNA, which is a trigger for innate immunity (85). Future studies of cellular responses via analysis of RNA changes following infection with toxic and nontoxic viruses, within different cell types, immediately and later after infection might reveal the primary responders as well as secondary effects. Follow-up studies using genetics in mice may further delineate the responsible pathways and cell types. Although not all studies conducted in mice can be extrapolated to other species, these data can provide a starting point for experiments that are more difficult to conduct in large animals and may be predictive of safer vector structures for human gene therapy.

Materials and Methods

Mice. CD-1 and C57BL/6J mice were purchased from Charles River Laboratories and were kept on a 12-h light/12-h dark cycle. All animal procedures performed were approved by the Institutional Animal Care and Use Committee of Harvard University and by Hong Kong Department of Health under Animals Ordinance Chapter 340, and animal care was carried out in accordance with institutional guidelines.

Plasmids. pAAV-CMV-GFP and pAAV-CMV-null vector plasmids were obtained from Harvard DF/HCC DNA Resource Core (pAAV-GFP and pAAV-MCS8 deposited by Jeng-Shin Lee to Harvard DF/HCC DNA Resource Core). pAAV-UbiC-GFP was made by replacing the CMV promoter in AAV-CMV-GFP with that of human UbiC from Addgene no. 11155 (21, 22, 77). pAAV-CAG-GFP (from the E. Boyden laboratory) was obtained from Addgene (Addgene no. 37825). pAAV-RedO-GFP, pAAV-Rho-GFP, and pAAV-CAR-GFP were gifts of the B. Roska laboratory, Friedrich Miescher Institute for Biomedical Research, Basel (29). pAAV-RK-ZsGreen was a gift from the T. Li laboratory, National Eye Institute, Bethesda, MD (31). pAAV-Best1-GFP was cloned by replacing the CMV promoter of the pAAV-CMV-GFP-BGHpA vector (Upenn virus core, ID: PV0101) with the −585/+39 bp region of human Best1 promoter region by Gibson ligation (27). pAAV-CMV-TdTomato were cloned by replacing GFP with TdTomato coding sequence by Gibson ligation. pAAV rep/Cap 2/2, 2/8 and Adenovirus helper plasmids were obtained from University of Pennsylvania Vector Core, Philadelphia. pAAV7m8 and pAAVAnc80 plasmids were gifts from J. Flannery, University of California, Berkeley, CA (2) and L. Vandenberghe, Harvard Medical School, Boston (3).

AAV Vector Production and Tittering. Recombinant AAV8 vectors were produced as previously described, and AAV7m8 vectors were produced using the same protocol as for AAV2 (86). Briefly, AAV vector, rep/cap packaging plasmid, and adenoviral helper plasmid were mixed with polyethylenimine and added to HEK293T cells (HCL4517; Thermo Scientific). Seventy-two hours after transfection, supernatant was collected for AAV8 preparations, and cells were harvested for AAV7m8 preparations (87). AAV8 viruses in the

supernatant were precipitated (mixed with 8.5% wt/vol PEG-6000 and 0.4 M NaCl for 2 h at 4 °C), centrifuged at 7,000 × *g* for 10 min, and resuspended in virus buffer (150 mM NaCl and 20 mM Tris, pH 8.0). For AAV7m8 viruses, the cell pellet was resuspended in virus buffer, followed by three cycles of freeze–thawing, and Dounce-homogenized. Cell debris was pelleted at 5,000 × *g* for 20 min, and the supernatant was run on an iodixanol gradient. Recovered AAV vectors were washed three times with PBS using Amicon 100K columns (EMD Millipore). RT-PCRs and protein gels were run to determine virus titers.

AAV Injection. Subretinal injection into P0 neonate eyes was performed as previously described (88, 89). Approximately 0.25 μL AAV was introduced into the subretinal space using a pulled angled glass pipette controlled by a FemtoJet (Eppendorf). The fellow eyes were uninjected for within-animal controls.

OCT. OCT images of mouse eyes were taken by a commercially available OCT2 system in combination with the MicronIV fundus imaging system (Phoenix Research Labs). Detailed procedures can be found in *SI Appendix*.

ERG. ERGs were performed in vivo with the Espion E3 System (Diagonsys LLC) as previously described (33, 90). An ERG protocol was created to characterize the rod and cone responses with a minimal number of flash steps based on our previous studies of wild-type mice (91, 92). Detailed procedures can be found in *SI Appendix*.

Optomotor Responses. The optomotor responses of mice were measured using the OptoMotry System (CerebralMechanics) with minor modifications, as previously described (33, 90). Detailed procedures can be found in *SI Appendix*.

Flow Cytometry. Retinas were dissected from adult CX3CR1$^{gfp/gfp}$ mice (The Jackson Laboratory), in which microglia are labeled with GFP (42). Detailed procedures can be found in *SI Appendix*.

Immunohistochemistry of Whole-Eye Mounts. After mice were killed with CO_2, eyes were enucleated, dissected from tendons and extraocular muscles, and fixed in 4% paraformaldehyde for 2 h at room temperature. The anterior segment, lens, and vitreous were then removed. The posterior segment eye cups were blocked with 4% heat-inactivated goat serum and 1% triton in PBS for 1 h at room temperature. Eye cups were then incubated in primary antibody (rabbit anti-cone arrestin; EMD Millipore AB15282) diluted 1:100 in the blocking buffer for 2 d, rinsed three times in PBS for 30 min each, and stained with secondary antibody solution containing donkey anti-rabbit Alexa Fluor 647 (Jackson ImmunoResearch) at 1:100 and phalloidin conjugated to Alexa Fluor 568 at 1:100 (ThermoFisher) for 2 d. Eye cups were rinsed three times again in PBS for 30 min each. Radial cuts were made to enable flat-mounting of the eyes on coverslips. The whole-eye mounts were then imaged on a Nikon T1 W1 Yokogawa spinning-disk microscope using a 20× objective.

Retinal Section and Histology. Eyes were enucleated, and retinae were dissected and fixed in 4% formaldehyde for 30 min at room temperature. Fixed retinae were cryoprotected in sucrose in PBS for a few hours and embedded in optical cutting temperature compound on dry ice. Sections (20 μm thick) were cut on a cryostat (Leica). Retinal sections or whole retinal cups were blocked in 5% BSA in PBST (PBS with 0.1% Triton X-100), stained with primary antibodies at 4 °C overnight, and washed three times with PBST. Primary antibodies used in this study included rabbit anti-red/green opsin (1:300, AB5405; EMD Millipore); goat anti-blue opsin (1:100, sc-14365; Santa Cruz Biotechnology Inc.); rabbit anti-GFAP (1:500, Z0344; DAKO); rabbit anti-Iba1 (1:1,000, PA5-21274; ThermoFisher), and rhodamine-conjugated and FITC-conjugated PNA (1:1,000; Vector Laboratories). Sections were stained using secondary antibodies, including donkey anti- rabbit CY3, donkey anti-rabbit Alexa Fluor 647, and donkey anti-goat Alexa Fluor 647 (all used at 1:1,000; Jackson ImmunoResearch), and were costained with DAPI in the dark for 2 h at room temperature and mounted in Fluoromount-G (SouthernBiotech). Images were taken using a 40× objective with Z-stacks on a Zeiss LSM780 confocal microscope. Images used for comparison between groups were taken side by side at the same confocal settings.

Statistics. Data were represented as mean ± SD in Figs. 1*C*, 2*B*, and 6 *B* and *C* and as mean ± SEM in Figs. 5 and 6*D*. Sample sizes were indicated for each experiment. One-way ANOVA analysis with Tukey test was performed to compare multiple groups, and unpaired Student's *t* test was performed to compare two groups. GraphPad Prism was used to perform statistical analysis and make figures.

ACKNOWLEDGMENTS. We thank Microscopy Resources on the North Quad (Harvard Medical School) for their assistance, Dr. Claudio Punzo (University of Massachusetts Medical School), and Dr. Ying Kai Chan (Harvard Medical School) for sharing unpublished data and discussions. This work was funded by Howard Hughes Medical Institute and Astellas Pharma Inc. (C.L.C.), City University of Hong Kong Grant 9610345 (to W.X.), Hong Kong Research Grants Council Grant 21105916 (to W.X.), National Natural Science Foundation of China Grant 81770937 (to W.X.), National Institutes of Health/National Eye Institute Grant K08-EY023993-05 (to D.M.W.), Massachusetts Lions Eye Research Fund, Iraty Award (D.M.W.), National Eye Institute Audacious Goals Initiatives Grant U01 EY025497 (to Y.X.), and a Howard Hughes Medical Institute Medical Student Fellowship (M.J.C.).

1. Gao G, et al. (2004) Clades of adeno-associated viruses are widely disseminated in human tissues. *J Virol* 78:6381–6388.
2. Dalkara D, et al. (2013) In vivo-directed evolution of a new adeno-associated virus for therapeutic outer retinal gene delivery from the vitreous. *Sci Transl Med* 5:189ra76.
3. Zinn E, et al. (2015) In silico reconstruction of the viral evolutionary lineage yields a potent gene therapy vector. *Cell Rep* 12:1056–1068.
4. Bainbridge JWB, et al. (2008) Effect of gene therapy on visual function in Leber's congenital amaurosis. *N Engl J Med* 358:2231–2239.
5. Hauswirth WW, et al. (2008) Treatment of Leber congenital amaurosis due to RPE65 mutations by ocular subretinal injection of adeno-associated virus gene vector: Short-term results of a phase I trial. *Hum Gene Ther* 19:979–990.
6. Maguire AM, et al. (2008) Safety and efficacy of gene transfer for Leber's congenital amaurosis. *N Engl J Med* 358:2240–2248.
7. Nathwani AC, et al. (2011) Adenovirus-associated virus vector-mediated gene transfer in hemophilia B. *N Engl J Med* 365:2357–2365.
8. Acland GM, et al. (2001) Gene therapy restores vision in a canine model of childhood blindness. *Nat Genet* 28:92–95.
9. Aguirre GD (2017) Concepts and strategies in retinal gene therapy. *Invest Ophthalmol Vis Sci* 58:5399–5411.
10. Taylor AW (2016) Ocular immune privilege and transplantation. *Front Immunol* 7:37.
11. Ghazi NG, et al. (2016) Treatment of retinitis pigmentosa due to MERTK mutations by ocular subretinal injection of adeno-associated virus gene vector: Results of a phase I trial. *Hum Genet* 135:327–343.
12. Lam BL, et al. (2019) Choroideremia gene therapy phase 2 clinical trial: 24-month results. *Am J Ophthalmol* 197:65–73.
13. Xue K, et al. (2018) Beneficial effects on vision in patients undergoing retinal gene therapy for choroideremia. *Nat Med* 24:1507–1512.
14. Mingozzi F, High KA (2013) Immune responses to AAV vectors: Overcoming barriers to successful gene therapy. *Blood* 122:23–36.
15. Hinderer C, et al. (2018) Severe toxicity in nonhuman primates and piglets following high-dose intravenous administration of an adeno-associated virus vector expressing human SMN. *Hum Gene Ther* 29:285–298.
16. Vandenberghe LH, et al. (2011) Dosage thresholds for AAV2 and AAV8 photoreceptor gene therapy in monkey. *Sci Transl Med* 3:88ra54.
17. Ramachandran PS, et al. (2017) Evaluation of dose and safety of AAV7m8 and AAV8BP2 in the non-human primate retina. *Hum Gene Ther* 28:154–167.
18. Khabou H, Cordeau C, Pacot L, Fisson S, Dalkara D (2018) Dosage thresholds and influence of transgene cassette in adeno-associated virus-related toxicity. *Hum Gene Ther* 29:1235–1241.
19. Gootwine E, et al. (2017) Safety and efficacy evaluation of rAAV2tYF-PR1.7-hCNGA3 vector delivered by subretinal injection in CNGA3 mutant achromatopsia sheep. *Hum Gene Ther Clin Dev* 28:96–107.
20. Reichel FF, et al.; RD-CURE Consortium (2017) AAV8 can induce innate and adaptive immune response in the primate eye. *Mol Ther* 25:2648–2660.
21. Bainbridge JWB, et al. (2015) Long-term effect of gene therapy on Leber's congenital amaurosis. *N Engl J Med* 372:1887–1897.
22. Dimopoulos IS, et al. (2018) Two-year results after AAV2-mediated gene therapy for choroideremia: The Alberta experience. *Am J Ophthalmol* 193:130–142.
23. Boshart M, et al. (1985) A very strong enhancer is located upstream of an immediate early gene of human cytomegalovirus. *Cell* 41:521–530.
24. Schorpp M, et al. (1996) The human ubiquitin C promoter directs high ubiquitous expression of transgenes in mice. *Nucleic Acids Res* 24:1787–1788.
25. Lois C, Hong EJ, Pease S, Brown EJ, Baltimore D (2002) Germline transmission and tissue-specific expression of transgenes delivered by lentiviral vectors. *Science* 295:868–872.
26. Niwa H, Yamamura K, Miyazaki J (1991) Efficient selection for high-expression transfectants with a novel eukaryotic vector. *Gene* 108:193–199.
27. Esumi N, Oshima Y, Li Y, Campochiaro PA, Zack DJ (2004) Analysis of the VMD2 promoter and implication of E-box binding factors in its regulation. *J Biol Chem* 279:19064–19073.
28. Wang Y, et al. (1992) A locus control region adjacent to the human red and green visual pigment genes. *Neuron* 9:429–440.
29. Busskamp V, et al. (2010) Genetic reactivation of cone photoreceptors restore visual responses in retinitis pigmentosa. *Science* 329:413–417.

30. Allocca M, et al. (2007) Novel adeno-associated virus serotypes efficiently transduce murine photoreceptors. *J Virol* 81:11372–11380.
31. Khani SC, et al. (2007) AAV-mediated expression targeting of rod and cone photoreceptors with a human rhodopsin kinase promoter. *Invest Ophthalmol Vis Sci* 48: 3954–3961.
32. Zhu X, et al. (2002) Mouse cone arrestin gene characterization: Promoter targets expression to cone photoreceptors. *FEBS Lett* 524:116–122.
33. Xiong W, MacColl Garfinkel AE, Li Y, Benowitz LI, Cepko CL (2015) NRF2 promotes neuronal survival in neurodegeneration and acute nerve damage. *J Clin Invest* 125: 1433–1445.
34. Constable IJ, et al. (2017) Gene therapy in neovascular age-related macular degeneration: Three-year follow-up of a phase 1 randomized dose escalation trial. *Am J Ophthalmol* 177:150–158.
35. Maguire AM, et al. (2009) Age-dependent effects of RPE65 gene therapy for Leber's congenital amaurosis: A phase 1 dose-escalation trial. *Lancet* 374:1597–1605.
36. Chang B, et al. (2006) Cone photoreceptor function loss-3, a novel mouse model of achromatopsia due to a mutation in Gnat2. *Invest Ophthalmol Vis Sci* 47:5017–5021.
37. Mattapallil MJ, et al. (2012) The Rd8 mutation of the Crb1 gene is present in vendor lines of C57BL/6N mice and embryonic stem cells, and confounds ocular induced mutant phenotypes. *Invest Ophthalmol Vis Sci* 53:2921–2927.
38. Vinberg F, et al. (2017) The Na^+/Ca^{2+}, K^+ exchanger NCKX4 is required for efficient cone-mediated vision. *eLife* 6:e24550.
39. Prusky GT, Alam NM, Beekman S, Douglas RM (2004) Rapid quantification of adult and developing mouse spatial vision using a virtual optomotor system. *Invest Ophthalmol Vis Sci* 45:4611–4616.
40. Silverman SM, Wong WT (2018) Microglia in the retina: Roles in development, maturity, and disease. *Annu Rev Vis Sci* 4:45–77.
41. Ito D, et al. (1998) Microglia-specific localisation of a novel calcium binding protein, Iba1. *Brain Res Mol Brain Res* 57:1–9.
42. Jung S, et al. (2000) Analysis of fractalkine receptor CX(3)CR1 function by targeted deletion and green fluorescent protein reporter gene insertion. *Mol Cell Biol* 20: 4106–4114.
43. Cideciyan AV, et al. (2008) Human gene therapy for RPE65 isomerase deficiency activates the retinoid cycle of vision but with slow rod kinetics. *Proc Natl Acad Sci USA* 105:15112–15117.
44. Feuer WJ, et al. (2016) Gene therapy for Leber hereditary optic neuropathy: Initial results. *Ophthalmology* 123:558–570.
45. Cukras C, et al. (2018) Retinal AAV8-RS1 gene therapy for X-linked retinoschisis: Initial findings from a phase I/IIa trial by intravitreal delivery. *Mol Ther* 26:2282–2294.
46. Hordeaux J, et al. (2018) Toxicology study of intra-cisterna magna adeno-associated virus 9 expressing human alpha-L-iduronidase in rhesus macaques. *Mol Ther Methods Clin Dev* 10:79–88.
47. Lock M, Alvira MR, Wilson JM (2012) Analysis of particle content of recombinant adeno-associated virus serotype 8 vectors by ion-exchange chromatography. *Hum Gene Ther Methods* 23:56–64.
48. Jabs DA, Nussenblatt RB, Rosenbaum JT; Standardization of Uveitis Nomenclature (SUN) Working Group (2005) Standardization of uveitis nomenclature for reporting clinical data. Results of the First International Workshop. *Am J Ophthalmol* 140: 509–516.
49. Xue K, Groppe M, Salvetti AP, MacLaren RE (2017) Technique of retinal gene therapy: Delivery of viral vector into the subretinal space. *Eye (Lond)* 31:1308–1316.
50. Li Y, Lowder C, Zhang X, Huang D (2013) Anterior chamber cell grading by optical coherence tomography. *Invest Ophthalmol Vis Sci* 54:258–265.
51. Ayuso E, et al. (2014) Manufacturing and characterization of a recombinant adeno-associated virus type 8 reference standard material. *Hum Gene Ther* 25:977–987.
52. Watanabe S, et al. (2013) Tropisms of AAV for subretinal delivery to the neonatal mouse retina and its application for in vivo rescue of developmental photoreceptor disorders. *PLoS One* 8:e54146.
53. Conlon TJ, et al. (2013) Preclinical potency and safety studies of an AAV2-mediated gene therapy vector for the treatment of *MERTK* associated retinitis pigmentosa. *Hum Gene Ther Clin Dev* 24:23–28.
54. Ai J, et al. (2018) Characterization of recombinant adeno-associated viral transduction and safety profiles in cdardiomyocytes. *Cell Physiol Biochem* 48:1894–1900.
55. Merentie M, et al. (2016) Efficacy and safety of myocardial gene transfer of adenovirus, adeno-associated virus and lentivirus vectors in the mouse heart. *Gene Ther* 23: 296–305.
56. Klein RL, et al. (2006) Efficient neuronal gene transfer with AAV8 leads to neurotoxic levels of tau or green fluorescent proteins. *Mol Ther* 13:517–527.
57. Watakabe A, et al. (2015) Comparative analyses of adeno-associated viral vector serotypes 1, 2, 5, 8 and 9 in marmoset, mouse and macaque cerebral cortex. *Neurosci Res* 93:144–157.
58. Ansari AM, et al. (2016) Cellular GFP toxicity and immunogenicity: Potential confounders in in vivo cell tracking experiments. *Stem Cell Rev* 12:553–559.
59. Liu H-S, Jan M-S, Chou C-K, Chen P-H, Ke N-J (1999) Is green fluorescent protein toxic to the living cells? *Biochem Biophys Res Commun* 260:712–717.
60. Loewendorf A, Benedict CA (2010) Modulation of host innate and adaptive immune defenses by cytomegalovirus: Timing is everything. *J Intern Med* 267:483–501.
61. Zhu J, Huang X, Yang Y (2009) The TLR9-MyD88 pathway is critical for adaptive immune responses to adeno-associated virus gene therapy vectors in mice. *J Clin Invest* 119:2388–2398.
62. Faust SM, et al. (2013) CpG-depleted adeno-associated virus vectors evade immune detection. *J Clin Invest* 123:2994–3001.
63. Hösel M, et al. (2012) Toll-like receptor 2-mediated innate immune response in human nonparenchymal liver cells toward adeno-associated viral vectors. *Hepatology* 55:287–297.
64. Martino AT, et al. (2011) The genome of self-complementary adeno-associated viral vectors increases Toll-like receptor 9-dependent innate immune responses in the liver. *Blood* 117:6459–6468.
65. Wu T, et al. (2012) Self-complementary AAVs induce more potent transgene product-specific immune responses compared to a single-stranded genome. *Mol Ther* 20: 572–579.
66. Kumar MV, Nagineni CN, Chin MS, Hooks JJ, Detrick B (2004) Innate immunity in the retina: Toll-like receptor (TLR) signaling in human retinal pigment epithelial cells. *J Neuroimmunol* 153:7–15.
67. Munoz-Erazo L, Natoli R, Provis JM, Madigan MC, King NJC (2012) Microarray analysis of gene expression in West Nile virus-infected human retinal pigment epithelium. *Mol Vis* 18:730–743.
68. Hadziahmetovic M, et al. (2012) Microarray analysis of murine retinal light damage reveals changes in iron regulatory, complement, and antioxidant genes in the neurosensory retina and isolated RPE. *Invest Ophthalmol Vis Sci* 53:5231–5241.
69. Jiang G, et al. (2009) Regulatory role of TLR ligands on the activation of autoreactive T cells by retinal astrocytes. *Invest Ophthalmol Vis Sci* 50:4769–4776.
70. Jiang G, Sun D, Kaplan HJ, Shao H (2012) Retinal astrocytes pretreated with NOD2 and TLR2 ligands activate uveitogenic T cells. *PLoS One* 7:e40510.
71. Kumar A, Shamsuddin N (2012) Retinal Muller glia initiate innate response to infectious stimuli via toll-like receptor signaling. *PLoS One* 7:e29830.
72. Kautzman AG, et al. (2018) Sox2 regulates astrocytic and vascular development in the retina. *Glia* 66:623–636.
73. Maclachlan TK, et al. (2011) Preclinical safety evaluation of AAV2-sFLT01- a gene therapy for age-related macular degeneration. *Mol Ther* 19:326–334.
74. Takahashi K, et al. (2017) Improved intravitreal AAV-mediated inner retinal gene transduction after surgical internal limiting membrane peeling in cynomolgus monkeys. *Mol Ther* 25:296–302.
75. Lannes N, Eppler E, Etemad S, Yotovski P, Filgueira L (2017) Microglia at center stage: A comprehensive review about the versatile and unique residential macrophages of the central nervous system. *Oncotarget* 8:114393–114413.
76. Rosario AM, et al. (2016) Microglia-specific targeting by novel capsid-modified AAV6 vectors. *Mol Ther Methods Clin Dev* 3:16026.
77. Kishi JY, Schaus TE, Gopalkrishnan N, Xuan F, Yin P (2018) Programmable autonomous synthesis of single-stranded DNA. *Nat Chem* 10:155–164.
78. Trotman LC, Mosberger N, Fornerod M, Stidwill RP, Greber UF (2001) Import of adenovirus DNA involves the nuclear pore complex receptor CAN/Nup214 and histone H1. *Nat Cell Biol* 3:1092–1100.
79. Cherry TJ, Trimarchi JM, Stadler MB, Cepko CL (2009) Development and diversification of retinal amacrine interneurons at single cell resolution. *Proc Natl Acad Sci USA* 106: 9495–9500.
80. Shekhar K, et al. (2016) Comprehensive classification of retinal bipolar neurons by single-cell transcriptomics. *Cell* 166:1308–1323.e30.
81. Trimarchi JM, et al. (2007) Molecular heterogeneity of developing retinal ganglion and amacrine cells revealed through single cell gene expression profiling. *J Comp Neurol* 502:1047–1065.
82. Trimarchi JM, Stadler MB, Cepko CL (2008) Individual retinal progenitor cells display extensive heterogeneity of gene expression. *PLoS One* 3:e1588.
83. Haberman RP, McCown TJ, Samulski RJ (2000) Novel transcriptional regulatory signals in the adeno-associated virus terminal repeat A/D junction element. *J Virol* 74: 8732–8739.
84. Flotte TR, et al. (1993) Expression of the cystic fibrosis transmembrane conductance regulator from a novel adeno-associated virus promoter. *J Biol Chem* 268:3781–3790.
85. Schlee M, Hartmann G (2016) Discriminating self from non-self in nucleic acid sensing. *Nat Rev Immunol* 16:566–580.
86. Grieger JC, Choi VW, Samulski RJ (2006) Production and characterization of adeno-associated viral vectors. *Nat Protoc* 1:1412–1428.
87. Vandenberghe LH, et al. (2010) Efficient serotype-dependent release of functional vector into the culture medium during adeno-associated virus manufacturing. *Hum Gene Ther* 21:1251–1257.
88. Matsuda T, Cepko CL (2004) Electroporation and RNA interference in the rodent retina in vivo and in vitro. *Proc Natl Acad Sci USA* 101:16–22.
89. Wang S, Sengel C, Emerson MM, Cepko CL (2014) A gene regulatory network controls the binary fate decision of rod and bipolar cells in the vertebrate retina. *Dev Cell* 30: 513–527.
90. Xue Y, et al. (2015) CRALBP supports the mammalian retinal visual cycle and cone vision. *J Clin Invest* 125:727–738.
91. Xue Y, Shen SQ, Corbo JC, Kefalov VJ (2015) Circadian and light-driven regulation of rod dark adaptation. *Sci Rep* 5:17616.
92. Xue Y, et al. (2017) The role of retinol dehydrogenase 10 in the cone visual cycle. *Sci Rep* 7:2390.